IN-SITU CALIBRATION OF INFRARED FILM COOLING MEASUREMENTS WITH THE SEED GAS CONCENTRATION TECHNIQUE

Patrick Jagerhofer
Graz University of Technology, Graz, Austria

ABSTRACT

This paper presents a novel hybrid approach to film cooling measurement, combining infrared (IR) thermography with the seed gas concentration technique. The seed gas concentration technique is used as an in-situ calibration ground truth for the IR measurements to correct for imperfect insulation and test facility-induced thermal disturbances, such as heat up of the coolant through viscous dissipation in the cavities as well as ingress and egress in the uncooled baseline case. This new approach allows the final film cooling results to inherit the advantages of both measurement techniques. The robustness against thermal disturbances, as well as the high accuracy, are inherited from the point-wise seed gas concentration technique, while the high spatial resolution is inherited from the full surface coverage IR measurements.

This new approach is demonstrated for purge film cooling measurements in a turbine center frame (TCF) tested under Mach-similarity in the transonic test turbine facility (TTTF) at Graz University of Technology. The TCF, also known as intermediate turbine diffuser, is a stationary duct that connects the high-pressure turbine (HPT) to the low-pressure turbine (TCF) in modern high-bypass ungeared turbofan engines. The TCF was operated in an engine-representative 1.5-stage test vehicle, where a fully purged HPT was operating upstream of the TCF and a row of LPT vanes was situated downstream of the TCF. The herein investigated sources of film cooling are the purge flows that emanate from the hub cavities of the HPT. These hub purge flows bear significant cooling potential for the downstream TCF hub surface. The TTTF is a good example to showcase the benefits of this new measurement approach as the complexity of the rig is high, and the challenging boundary conditions imposed on the technique are representative of many continuously operated and high technology readiness level (TRL) turbine test facilities.

NOMENCLATURE

c	strut chord length (m)
	seed gas concentration (CO_2 or N_2O)
D	molecular mass diffusivity (mm²/s)
DR	density ratio (= ρ_P/ρ_M)
I	momentum flux ratio (= $\rho_P V_P^2/\rho_M V_M^2$)
L	axial length of TCF (m)
M	blowing ratio (= $\rho_P V_P/\rho_M V_M$)
Ma	Mach number
$\dot{m}$	mass flow rate (kg/s)
n	rotational speed (rpm)
Re_c	Reynolds number based on strut chord length (= $V_\infty c/\nu$)
T	temperature (K)
U_F	uncertainty in parameter F
V	absolute velocity (m/s)
α	molecular thermal diffusivity (mm²/s)
ε	emissivity
	turbulent diffusivity
η	adiabatic film cooling effectiveness
ν	kinematic viscosity (m^2/s)
π	total pressure ratio
ρ	density (kg/m^3)
τ	transmissivity

Subscripts

ad	(quasi) adiabatic	r	recovery
IR	from infrared	W	window
M	mainstream	∞	freestream
NP	no purge	S	surface
P	purge	SG	from seed gas

1. INTRODUCTION

The measurement techniques for the adiabatic film cooling effectiveness can be categorized into thermal and mass transfer methods [1].

1.1. Thermal Methods

The thermal methods commonly work by measuring the film cooled surface temperature distribution and nondimensionalizing it with the coolant and the main flow temperature:

$$\eta = \frac{T_{r,\infty} - T_{S,ad}}{T_{r,\infty} - T_P} \quad (1)$$

Here, $T_{r,\infty}$ is the main flow recovery temperature, $T_{S,ad}$ is the film cooled adiabatic surface temperature, and T_P is the coolant, or in this work, purge temperature. In most cases for T_P, a distinction between static or recovery temperature is not necessary due to the low velocity of the coolant or purge flow.

As the name already says, the adiabatic film cooling effectiveness, η, assumes an adiabatic wall. However, all thermal techniques for measuring the adiabatic film cooling effectiveness are never truly adiabatic, as perfect insulators do not exist. Furthermore, test facilities that can cater high TRLs in turbomachinery are an extremely challenging environment for temperature measurements. For

instance, viscous dissipation of the rotating discs heats the coolant in the wheelspace cavities, falsifying the T_P measurement. Furthermore, ingress-egress patterns at the cavity exit are found [2], further complicating the thermal evaluation of η. Not all flow-wetted components can be made from insulating materials for safety reasons, or tradeoffs must be made between structural integrity and insulating properties. For instance, Hänni et al. [3] used PEEK (polyether-ether-ketone) as an insulating substrate on a rotor hub. PEEK was able to withstand the centrifugal loads but at the price of higher thermal conductivity compared to foam materials with less strength, such as PMI (polymethacrylimide). In addition, most film-cooled surfaces are cooled by multiple coolant injections and sometimes purged from multiple slots with different coolant and purge temperatures. The well-known superposition formula of Sellers et al. [4] allows to combine multiple effictivenesses, but the coolant temperatures need to be equal. If this is the case, the Sellers superposition can be used not only for flat plate applications but also for turbomachinery-relevant geometries, as shown by Muska et al. [5].

It can be concluded that the idealized boundary conditions needed for most thermal film cooling measurement techniques are only found in simple flat plate or linear cascade test facilities. Consequently, cutbacks in measurement quality or accuracy are inevitable when such thermal methods are transferred to a high TRL test facility.

In state-of-the-art setups, $T_{S,ad}$ is typically a 2D temperature distribution that has to be acquired. Available techniques to measure 2D temperature distributions include infrared (IR) thermography [6], thermochromic liquid crystals (TLC) [7] and for high temperature applications, thermal history coatings and paints [8]. All techniques share the above-mentioned challenges but also have their own strengths and weaknesses compared to each other. Thermal history coatings and paints have a minimum working temperature of 150°C [7], which is too high for film cooling investigations in most cold flow facilities but ideal for real gas turbine applications. IR thermography has the widest possible temperature range and is theoretically non-invasive. The main challenge is the transition from qualitative to quantitative measurements. The surface emissivity and temperature of the surroundings must be known, and humidity must be addressed if the measurement target is far away from the camera. When using an IR window, its transmissivity and temperature must be measured. The emissivity on curved surfaces cannot be considered to remain constant over the viewing angle [9]. The same is true for the window transmissivity. Consequently, the calibration effort disproportionally increases with the complexity of the setup, and in-situ temperature measurements [10], [11] are often necessary, making the technique invasive. TLC coatings or paints can be tailored to the specific application in the range from -30°C to 120°C [7] with very competitive accuracies. However, such high accuracies can only be achieved with extensive calibration and rigorous consistency requirements between calibration and measurement. In practice, an in-situ calibration with thermocouples is often required, as for instance in the work of Barigozzi et al. [12]. This also makes the TLC technique invasive. Further challenges in high TRL facilities include ageing and hysteresis of the TLC [7] and higher optical access requirements than for IR thermography due to the need for uniform illumination. Consequently, the choice of the correct temperature measurement technique depends on the test facility. The technique herein chosen and best suited is IR thermography due to limited optical access and harsh operating conditions.

1.2. Mass Transfer Methods

Mass transfer methods facilitate the heat and mass transfer analogy and, thus, are inherently truly adiabatic. However, the validity of the heat and mass transfer analogy ultimately depends if the unit-Lewis-number assumption [13] holds for the mass transfer technique and the test setup in question. The Lewis number equals the Prandl over the Schmidt number and can be seen as the fraction of molecular mass over molecular thermal diffusivity:

$$Le = \frac{D}{\alpha} = \frac{Pr}{Sc} = \frac{mass\ diffusivity}{thermal\ diffusivity} \qquad (2)$$

For instance, for the seed gas concentration technique with 8% CO_2 seeding Le ≈ 0.77 and for the naphthalene sublimation technique Le ≈ 0.31 [14]. Caution is therefore required in the laminar regime, particularly when dealing with gases with very different characteristics than air, because the unit-Lewis-number assumption may not hold. Kulkarni et al. [14] examined analogy-conversion factors for naphthalene sublimation, transforming the mass transfer coefficient into the heat transfer coefficient. In gas turbines, the turbulence is typically high enough that the unit-Lewis-number assumption is valid [13]. In the turbulent case, the turbulent mass and heat diffusion coefficients, ε_{mass} and ε_{heat}, are added to their molecular counterparts, D and α, in Eq. (2) [15]. This fraction is usually very close to unity in gas turbines because the turbulent diffusion coefficients are similar to each other and significantly larger than the molecular diffusivities:

$$\frac{D + \varepsilon_{mass}}{\alpha + \varepsilon_{heat}} \approx 1 \qquad (3)$$

In other words, film cooling problems in turbomachinery are predominantly mixing problems, as advective mechanisms dominate over diffusive mechanisms. If the above conditions are met, temperatures can be replaced with concentrations in Eq. (1):

$$\eta = \frac{T_{r,\infty} - T_{S,ad}}{T_{r,\infty} - T_P} = \frac{c_\infty - c_S}{c_\infty - c_P} \qquad (4)$$

Even if the unit-Lewis-number assumption holds, mass transfer techniques have their own challenges, and their implementation into a high TRL facility can also be challenging. For instance, the pressure-sensitive paint (PSP) technique needs a large optical access for camera and illumination as well as heavy calibration to account for the numerous cross-dependencies of the paint [16]. Furthermore, PSP ages significantly under ultraviolet light [17], which is often used to excite it. The seed gas concentration technique is a 1D method and, therefore, requires numerous static wall pressure taps to achieve a useful spatial resolution. However, the seed gas technique has no cross-dependencies and delivers the highest accuracy possible. For instance, Patinios et al. [18] reported uncertainties in η as low as ±0.005 using CO_2 as a foreign gas and an infrared gas analyzer. The naphthalene sublimation, as well as the ammonia and diazo technique, mandatorily require a constant main flow temperature [19], [20], which is in a high TRL facility virtually impossible as the outlet of a combustor or HPT is never isothermal.

The seed gas concentration technique is typically the most suitable mass transfer method for stationary parts, such as nozzle guide vanes, stator rows and TCFs, in high TRL facilities. Often, arrays of wall pressure taps already exist for static pressure measurements. If this is the case, no additional instrumentation is necessary at the test vehicle. No optical access is needed, and the addition of foreign gases to the coolants can be done far upstream in the supply pipes of the test vehicle. The gas samples can be drawn from the conventional pressure tubes, and the gas analyzer can be conveniently placed next to the pressure transducer, making this technique "drop-in" capable.

2. EXPERIMENTAL FACILITY

This section presents the transonic test turbine facility (TTTF) and the instrumentation with the test vehicle.

2.1. Test facility

The TTTF is a continuously operated, open circuit, cold-flow and Mach-similar test turbine facility. The main flow temperatures of the facility range, depending on the test vehicle, from ambient to approx. 160°C. As shown in the flow schematic in Fig. 1, the TTTF is supplied with pressurized air from a 3 MW compressor station (CS). The HPT drives a brake compressor (BC) that returns the compressed air through a mixing chamber (MC) to the HPT inlet, thereby recuperating the HPT power. Downstream of the TTTF, a 0.6 MW suction blower (SB) is used to boost the overall pressure ratio of the facility and decouple the outlet pressure from ambient variations. The HPT has four purge flow injections fed from an auxiliary 1.1 MW compressor station (Aux. CS). The purge flows are temperature and massflow conditioned in the secondary air system (SAS), thoroughly described in Steiner et al. [21]. The rough working principle of the SAS is that the four purge flows are mixed from a hot and a cold reservoir using two needle valves for each purge flow. Depending on the valve settings, purge supply temperatures vary approx. between 10°C and 33°C.

2.2. Test vehicle

The test vehicle, shown in Fig. 2, is a 1.5-stage HPT-TCF-LPT vane setup and was operated by setting the corrected HPT speed, HPT pressure ratio and turbine inlet temperature to reach Mach-similarity and similar velocity triangles. By setting a constant outlet pressure with the suction blower (SB), the corrected massflow is automatically set and consistent between different test runs.

The unshrouded HPT is aerodynamically representative of the second stage of a turbofan's state-of-the-art HPT. Here in this facility, the HPT has no cooling holes or trailing edge cooling but is fully purged. The overall four purge flow injections are illustrated in Fig. 2. On the hub, the purge flows are fed into the forward (FWD) and aft (AFT) wheelspace cavities and are then injected through product-representative rim seals into the main flow. These hub purge flows are the coolant sources for the herein-demonstrated film cooling measurements. At the tip, the purge flows are fed into the FWD and AFT tip cavities and then injected into the main flow through axial slots. The tip purge flows are not investigated here.

The HPT is followed by the TCF, which is the focus of the film cooling measurements in this study. The target measurand is the purge film cooling effectiveness on the TCF hub and strut surfaces.

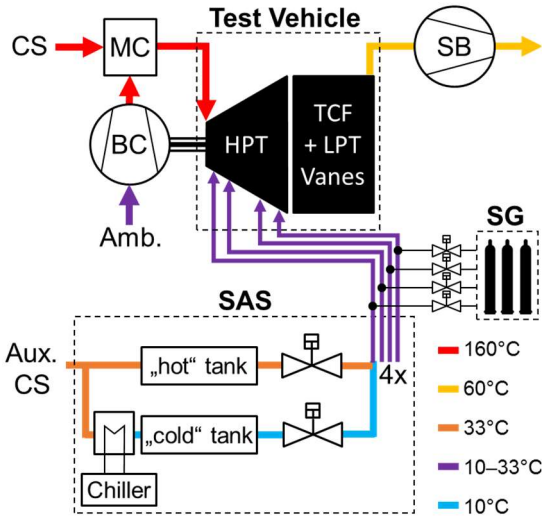

Fig. 1 Flow schematic of the transonic test turbine facility (TTTF) during normal operation

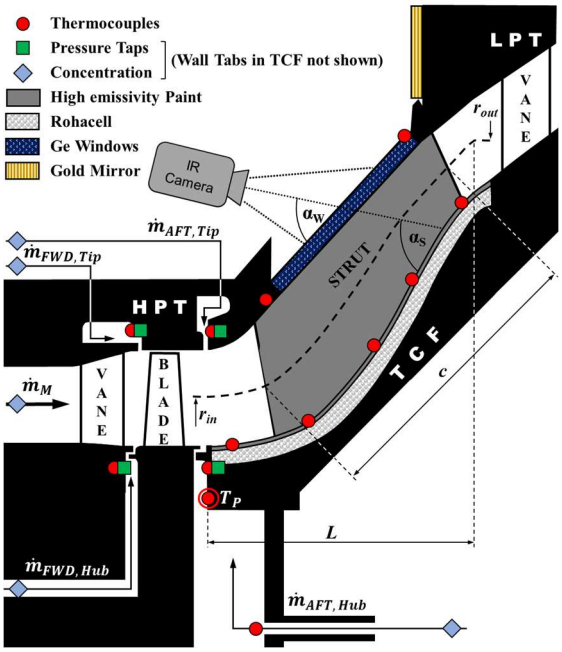

Fig. 2 Cross section of the test vehicle (adapted from Jagerhofer et al. [22])

The TCF is aerodynamically very aggressive with a radial offset relative to its axial length, $\Delta r/L$, significantly higher than 0.5. This leads to pronounced bends on the hub (inner casing) and the shroud (outer casing). The TCF has twelve so-called struts, which are thick non-turning airfoils. The HPT vane to TCF strut count is exactly four, making the flow field periodic and identical in every TCF passage. The TCF is followed by a row of LPT vanes for a realistic outlet condition.

2.3. Instrumentation

Fig. 2 also shows the instrumentation of the test vehicle for the purge film cooling measurements. In all four cavities, at least three circumferentially equidistant distributed thermocouples, indicated by red circles, and pressure taps, indicated by green squares, were placed to monitor the purge flows. The AFT hub cavity was instrumented more intensively with thermocouples at three different radial heights, the first at the lowest radius right at the purge injection into the wheelspace, the second at some distance from the rim seal and the third right inbound from the rim seal. The seed gas concentrations, indicated by blue diamonds, of all four purge flows were drawn from the purge supply lines far upstream. The seed gas concentration of the main flow was drawn from a wall pressure tap upstream of the HPT.

The herein-used thermal measurement technique is IR thermography. A FLIR T650sc IR camera with an uncooled microbolometer sensor with a high sensitivity of 20 mK was used. The optical access was enabled into one TCF passage by two trapezoidal broad-band anti-reflective coated germanium windows (BBAR-GE) placed in the shroud casing of the TCF. To avoid any aerodynamic interference from the flat GE windows, the size and placement of the windows were limited to the area where the TCF shroud contour was relatively straight. To observe the whole hub and both strut surfaces, the IR camera had to be moved to 21 different positions using a 5-axis traversing system. For regions on the TCF hub very close to the AFT hub cavity exit, a gold mirror was required to provide optical access for the camera. To further increase the achievable IR temperature measurement accuracy, overall 15 in-situ thermocouples were distributed over the investigated surfaces. The five in-situ thermocouples along the hub centerline are indicated as red circles in Fig. 2. Furthermore, the TCF shroud temperature, which is driving the reflected background radiation, and the GE window temperature, which also needs to be known, was measured with thermocouples as well. All thermocouples were individually calibrated before installation in the test vehicle.

Since the target measurand is the adiabatic film cooling effectiveness, a quasi-adiabatic PMI foam with a thermal conductivity of 0.043 W/mK (Rohacell Hero 200) was used to reduce the conductivity of the investigated surfaces to a minimum. On the hub, a 1cm thick PMI foam insert was used. The two struts of this thermal TCF passage were milled from PMI foam with a thin structural metal core. On top of the PMI foam parts, thin heating foils were glued. These foils were not used for this study and remained switched off during the measurements. These foils were spray painted with the high emissivity paint Nextel Velvet 811-21.

Close to the thermally instrumented TCF passage, shown in Fig. 2, another instrumented passage exists with a very high density of wall pressure taps. This pressure tap sector is shown as top view in Fig. 3, and all taps are illustrated as blue diamonds. Overall 60 pressure taps were placed on the hub, where the instrumentation density was increased towards the AFT hub cavity exit.

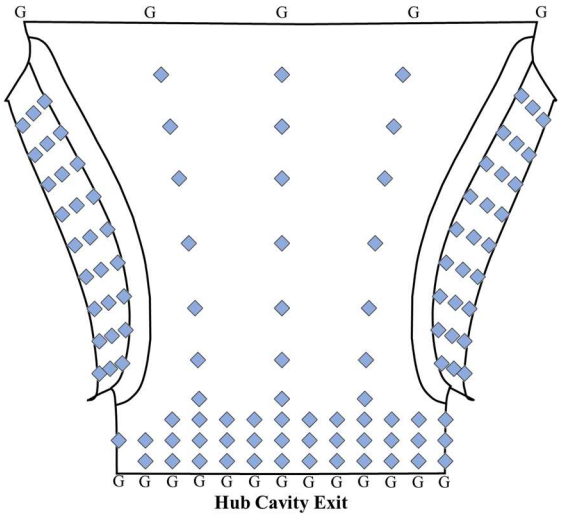

Fig. 3 Pressure taps on TCF hub and struts

Unfortunately, three hub pressure taps got clogged during the final assembly and are, therefore, not shown in Fig. 3. On the struts, 27 pressure taps were placed per strut side. This makes a total of 111 usable pressure taps in this setup.

2.4. Operating point

The operating point, given in Table 1, is reused here from Jagerhofer et al. [22] to showcase the measurement technique. The nominal purge case is aerodynamically nominal to engine operation. The no purge case is, as will be explained later, a necessary baseline case for the thermal film cooling measurements. As shown in Jagerhofer et al. [22], the purge blowing ratios are low enough that the purge flows operate most likely in the density ratio-insensitive regime. In other words, not matching the density ratio to the engine conditions for the given low blowing ratios of the purge flows does not significantly affect flow physics because the cooling films are fully attached in the real engine as well as in the test facility. This observation is consistent with the work of Sinha et al. [23] and the conclusions drawn in the review of Bogard and Thole [1] for blowing ratios lower than 0.5 or 0.2, respectively.

3. MEASUREMENT TECHNIQUE

The herein-presented new approach to film cooling measurements relies on the combination of IR thermography with the seed gas concentration technique.

Table 1: Operating conditions

Operating Parameter		Test Case	
		No Purge	Nominal Purge
Mach number at TCF inlet, Ma		0.5	(±1%)
Rotational speed HPT, n		9600 rpm	(±0.1%)
Main mass flow, $\dot{m}_M$		13.2 kg/s	(±2%)
Rig total pressure ratio, π_{Rig}		2.6	(±0.5%)
Reynolds number, Re_c		$>10^6$	(±1%)
FWD Hub	Blowing ratio, M	0	0.25
	Density ratio, DR	-	1.46
	Momentum flux ratio, I	0	0.043
AFT Hub	Blowing ratio, M	0	0.11
	Density ratio, DR	-	1.05
	Momentum flux ratio, I	0	0.012
FWD Tip	Blowing ratio, M	0	0.59
	Density ratio, DR	-	1.70
	Momentum flux ratio, I	0	0.203
AFT Tip	Blowing ratio, M	0	0.23
	Density ratio, DR	-	1.02
	Momentum flux ratio, I	0	0.052

First, the IR measurement and data reduction are described, then the seed gas technique is presented, and finally, the combination of both techniques into the final η results is explained.

3.1. Infrared technique

The explanation of the calibrations and the data reduction is kept short in this section, as the working principle of the IR film cooling measurement technique was already explained extensively in the open-access publication Jagerhofer et al. [24].
Altogether 21 IR images are necessary to cover the whole hub and both strut surfaces. These raw IR images undergo a sequence of postprocessing and calibration steps. First, every raw IR image is 2D-3D mapped onto a structured surface mesh of the TCF and all unwanted pixels, i.e. the window frame, are rejected. Second, a three-step pre-calibration is applied to correct the camera's inherent error and the viewing angle dependencies of the high emissivity paint and the IR window. These angular calibrations are necessary because the limited optical access, together with the strong curvature of the hub and strut surfaces, lead to very shallow surface and window viewing angles, α_S and α_W. Consequently, ε_S cannot be assumed to be constant but a function of the viewing angle, α_S. The same is true for τ_W; it becomes a function of α_W. These angular dependencies are given in Fig. 4.

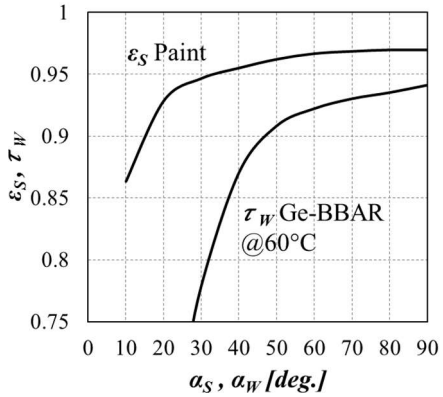

Fig. 4 Paint emissivity and GE window transmissivity as a function of surface and window angle, respectively. (adapted from [22])

After the 2D-3D mapping and the pre-calibrations, the 21 temperature patches must be overlapped to form a full surface coverage temperature distribution. Finally, this temperature distribution is then in-situ calibrated with the overall 15 surface thermocouples to maximize the achievable measurement accuracy. The final result is a fully calibrated surface temperature distribution that covers the entire hub and the struts to up to 80% channel height.

The total temperature distribution at an HPT outlet is not constant. In the case of the herein investigated test vehicle, total temperature variations at the HPT outlet (=TCF inlet) of around

10K can be found. Without purge flows, these total temperature differences will imprint onto the TCF surfaces with a recovery factor of approx. 0.9 [25]. Consequently, it is not sufficient to use a single scalar value for $T_{r,\infty}$ in Eq. (1) downstream of an HPT. Instead, $T_{r,\infty}$ has to be replaced with a full surface coverage measurement of the adiabatic surface temperature when the purge flows are switched off:

$$\eta_{IR} = \frac{T_{S,ad,NP} - T_{S,ad,P}}{T_{S,ad,NP} - T_P} \quad (5)$$

Here, $T_{S,ad,P}$ is the purged and $T_{S,ad,NP}$ is the non-purged quasi-adiabatic temperature distribution along the hub and strut surfaces, both postprocessed as described above. These final temperature distributions are saved on the structured surface mesh with a resolution of 500,000 cells.

The need for a no purge measurement invokes a new challenge. In a simple flat plate facility, the coolant can be switched off without changing the operating point. With an HPT, however, switching off one or both hub purge flows alone would cause the rotor disc to heat up and thermally expand in the still cooled casing. Consequently, the tip clearance would shrink, and the operating point consistency would be lost. Therefore, all four purge flows must be turned off to allow the rotor and the casing to expand thermally together. In this way, the tip clearance and, thus, the operating point can be held consistent between the purged and the non-purged case.

Three further challenges lie in the definition of the purge temperature, T_P, in Eq. (5). First, when both hub purge flows are switched off to acquire $T_{S,ad,NP}$, η_{IR} is, per definition, the combined film cooling effectiveness of the FWD and AFT hub purge flows. Here, the assumption has to be made that the AFT hub purge flow dominates the cooling effect, and therefore, the AFT hub purge temperature is defined as T_P. Second, the definition of T_P inside a rotating wheelspace cavity is not trivial. The purge flow heats up significantly due to viscous dissipation as it passes radially outwards towards the rim seal. In the herein investigated test vehicle, the AFT hub purge flow heated up by more than 30K inside the wheelspace. Third, the AFT hub cavity is not entirely sealed at nominal purge mass flows, as is normally also the case in real engines. The ingress into the AFT hub cavity was investigated using the seed gas concentration technique similar as in the work of Patinios et al. [26]. However, only the following statements can be given on the cavity ingress due to confidentiality agreements on this data: A small but noticeable ingress of hot mainstream gas occurs at the position of the radially highest row of thermocouples in the AFT hub cavity. For this reason, the radially next lower row of thermocouples was defined as the measurement point for T_P, as indicated in Fig. 2. This position represents a good compromise, as most of the dissipation heating has already occurred, and no notable ingress was found at this radius.

Ultimately, the definition of T_P decides if certain flow phenomena are considered to be part of the film cooling problem or not. In the end, this decision is up to the experimentalist. In other words, the definition of T_P draws the system boundaries of the film cooling problem. For instance, if T_P was defined at the lowest thermocouple right at the injection, the film cooling problem would include the viscous dissipation in the wheelspace and the ingress-induced pre-mixing of purge with main flow inside the cavity. If T_P was defined at the radially highest thermocouple, viscous dissipation and a part of the ingress-induced pre-mixing would be excluded. In the current definition, shown in Fig. 2, most of the viscous dissipation is excluded, but all of the ingress-induced pre-mixing is included in the film cooling problem. This definition was chosen because it is physically most consistent with the seed gas concentration technique, as will be shown later.

As can be seen, compromises, assumptions, and heavy adaptions to the test vehicle are necessary to incorporate a thermal film cooling measurement technique into a high TRL test facility. The difficulties in the definition of T_P and the difficulties arising from having a non-constant mainstream recovery temperature, $T_{r,\infty}$, are common in all thermal techniques and not limited to IR thermography.

3.2. Seed gas concentration technique

The seed gas concentration technique was first applied in the TTTF in the work of Patinios et al. [18] and is thoroughly described there. In Summary, it is a mass transfer method where a foreign gas is added with a known concentration, $c_{P,}$ to one purge flow, and the concentration of this foreign gas is then measured on the investigated surfaces by drawing gas samples from the wall pressure taps, shown in Fig. 3. The foreign gas concentration from these samples, c_S, is analyzed using a two-channel Siemens Ultramat 6E gas analyzer. This analyzer uses the non-dispersive infrared (NDIR) measurement principle. The two channels of the analyzer allow the use of two different foreign gases simultaneously, which, in turn, allows for halving the measurement time and still acquiring the individual cooling impact of both hub purge flows. The FWD hub purge flow was seeded with 5% $CO_{2,}$ and the AFT hub purge flow was seeded with 5% N_2O. These two foreign gases were selected because they have the same gas constant and non-overlapping IR absorption spectra. In addition, the absorption spectra of both foreign gases do also not overlap with the spectral range of the IR camera so that the thermal and mass transfer film cooling measurements can take place simultaneously.

With maximum foreign gas concentrations of 5% and the highly turbulent flow downstream the HPT, the unit-Lewis-number assumption in Eq. (3) holds, and the film cooling effectiveness from the seed gas measurement reads:

$$\eta_{SG,FWD/AFT} = \frac{c_S - c_\infty}{c_P - c_\infty} \quad (6)$$

The CO_2 concentration is measured for the film cooling effectiveness of the FWD hub purge flow and the N_2O concentration for the AFT hub purge flow.

The FWD and AFT film cooling effectiveness are then combined using the well-known formula of Sellers [4]:

$$\eta_{SG} = 1 - (1 - \eta_{SG,FWD})(1 - \eta_{SG,AFT}) \quad (7)$$

Strictly speaking, the concentrations in Eq. (6) are mass fractions, but the concentrations measured by the gas analyzer are volume fractions. For the given species and the low seeding concentrations of 5%, the error from assuming the mass and the volume fraction to be equal is always less than 0.0064 in absolute units of η and, therefore, negligible. However, care must be taken when using a higher seeding concentration or a foreign gas with a molecular weight significantly different from air.

Another often overlooked source of error when incorporating the seed gas technique into an existing facility is the purge (or coolant) mass flow measurement system. By adding a foreign gas, the properties, i.e. the gas constant, of the purge (or coolant) are changed. Depending on the method used to measure the mass flow, this may result in erroneous mass flow readings if corrections are not made.

If the points above have been considered, the seed gas concentration technique is a very robust and accurate film cooling measurement technique. The foreign gas concentration is neither influenced by thermal conduction nor viscous dissipation heating in the rotating wheelspace cavity. However, the ingress-induced pre-mixing of the purge flow is sensed by the seed gas concentration technique, which now justifies the T_P definition above.

One could argue that the viscous heating of the purge flow should also be included in the film cooling problem, as the same process occurs in the real engine. If the rotor speed is similar, the heat pick-up in ΔT is roughly comparable in the real engine and in the test facility. However, a, for instance, 30K heat pick-up is very significant for the temperature differences in a cold flow facility but insignificant for hot gas temperatures of ≈1300K with coolant temperatures of ≈700K. Therefore, the experiment was designed here to exclude the viscous heating from the measurements.

3.3. Calibrating the IR with the seed gas data

After conducting the thermal and mass transfer measurements, η_{IR} is available as full surface coverage distribution on the ordered surface mesh. However, η_{SG} is only available at the discrete points of the wall pressure taps. Since the seed gas data is more accurate and robust, it will be used as a point-wise in-situ calibration ground truth for the IR data as follows: First, the in-situ offset is calculated at the 111 discrete positions of the wall pressure taps.

$$\Delta\eta_{in-situ} = \eta_{SG} - \eta_{IR} \quad (8)$$

Second, this point-wise in-situ offset data is turned into a full surface coverage "delta field" using the natural neighbour interpolation [27]. Since the natural neighbour interpolation is strictly an interpolation method, the regions outside the pressure taps must be treated differently. If the extrapolation region is relatively small, a linear extrapolation is sufficient. Here, the extrapolation region is considered too large and so-called ghost points, marked as "G" in Fig. 3, were introduced to extend the interpolation region artificially. The $\Delta\eta_{in\text{-}situ}$ value of the closest pressure tap was assigned to each ghost point. When there was no clear closest pressure tap, as it is the case for the front left corner at the hub cavity exit and both corners at the TCF outlet, the average $\Delta\eta_{in\text{-}situ}$ of the two closest pressure taps was assigned to the ghost point. With the help of the ghost points, the natural neighbour interpolation can be used along the whole hub and strut surface mesh.

After the interpolation, $\Delta\eta_{in\text{-}situ}$ is available at every cell of the surface mesh and can be added to the η_{IR} distribution on a cell-by-cell basis to obtain the final film cooling effectiveness distribution:

$$\eta_{final} = \eta_{IR} + \Delta\eta_{in-situ} \quad (9)$$

The key feature of the method is that Eq. 8 is only carried out at the discrete positions of the wall pressure taps, but Eq. 9 is carried out over the entire surface mesh in all cells. At a wall pressure tap, combining Eq. 8 and 9 cancels η_{IR} out and $\eta_{final}=\eta_{SG}$. Between the pressure taps, however, the in-situ offset is interpolated, and the features in the IR measurement are preserved. This allows to combine the seed gas technique's robustness and accuracy with the IR technique's high spatial resolution.

4. RESULTS AND DISCUSSION

Fig. 5 shows top views of the TCF hub and strut surfaces, whereas the flow direction is from bottom to top, and the AFT hub cavity exit is located at the position of the letters (a)-(d). Fig. 5 always deals with the combined film cooling effectiveness emanating from the FWD and the AFT hub purge flows. It should be stated in advance that the AFT hub purge flow is the main contributor to the film cooling effectiveness on the TCF hub.

The film cooling effectiveness measured with infrared thermography is shown in Fig. 5 (a). The spatial coverage extends over the whole hub surface and both struts surfaces until approx. 80% channel height. On the hub at the TCF outlet, two white spots without data exist due to a small coating ablation on one GE window that blocked the optical access in this area. The average spatial resolution of the η_{IR} data is approx. 4 data points per mm.

In the η_{IR} field, longitudinal streaks of higher film cooling effectiveness can be seen. These streaks are real and not an artefact from the infrared measurement technique. The streaks are formed in the wakes of the HPT vanes because the total pressure and static wall pressure are lower in the HPT vane wakes. Since there are four HPT vanes per TCF passage, there are also four high film cooling streaks in one TCF passage. More on the physical formation of the longitudinal film cooling streaks is given in Jagerhofer et al. [22]. However, the circumferential η_{IR} distribution right at the cavity exit is unphysical. The shape of the cooling film there might lead to the false conclusion that the upstream blockage of the TCF struts is excessively strong, and the coolant exits the cavity as one concentrated plume between the struts. However, wall static pressure measurements, presented in [22], showed only a marginal upstream blockage effect of the struts and the η_{SG} distribution in (b) also looks vastly different close to the cavity exit. The explanation for this concentrated plume of seemingly high film cooling effectiveness is the combination of reduced IR measurement accuracy in this region and an ingress-egress pattern in the no purge case. The reduced IR measurement accuracy close to the cavity exit comes from the very limited optical access, the necessity to use the gold mirror for this region and very shallow surface and window viewing angles, as can be seen in Fig. 2. In the no purge case, which is necessary for the evaluation of η_{IR}, a small amount of main flow ingresses into the AFT hub cavity in front of the struts, heats up in the cavity through viscous dissipation and then exits (or egresses) as hotter fluid back into the main flow between the struts. This impacts the $T_{S,ad,NP}$ distribution and, hence, contributes to this concentrated plume of seemingly high film cooling effectiveness close to the cavity exit. As can be seen, infrared film cooling measurements deliver very high spatial resolution, but a manifold of error sources exist in high TRL facilities that need to be addressed.

Fig. 5 (b) shows the combined film cooling effectiveness, calculated from Eq. (7) and measured with the seed gas concentration technique. As mentioned above, this data only exists point-wise at the wall static pressure taps, where the gas samples were drawn from, shown as black dots. The distribution shown here was obtained by natural neighbour interpolating the point-wise η_{SG} data.

It is important to note that this interpolated distribution is used here only to present the seed gas data, but it was not used for in-situ calibrating the infrared measurements. As mentioned above, the in-situ offset between η_{SG} and η_{IR} must be determined only at the positions of the pressure taps, and only then the point-wise offset data is interpolated and used for further data processing. The correct order of offset calculation and interpolation is crucial to this measurement technique.

The four longitudinal film cooling streaks are also clearly evident in the η_{SG} distribution. However, after the first three circumferential rows of pressure taps, the pressure tap density decreases and is then too coarse to detect the streaks in this downstream region. The film cooling effectiveness on both strut surfaces is always below 0.05 and, therefore, negligible.

Fig. 5 (c) is the natural neighbour interpolated $\Delta\eta_{in\text{-}situ}$ field. The wall pressure taps are again shown as black dots, and the ghost points are indicated as pink dots. The average value of the offset field is -0.045 and, thus, very close to zero, which shows that the IR technique gives correct results on average and that the choice of the T_P measurement position was adequate. Close to the hub cavity exit, an alternating positive-negative offset pattern exists that matches the shape, number and position of the longitudinal film cooling streaks. It appears that the infrared technique underestimates the intensity of the film cooling streaks right after the cavity exit. In this region, the highest lateral temperature gradient exists, which drives lateral redistribution of heat (conduction) and, consequently, blurs out the intensity of the streaks. The heating foils, which were not used in this study but were situated on top of the insulating substrate, appear to be sufficiently thermally conductive to cause this lateral conduction. This was somewhat surprising as the copper layer in the heating foils was only 0.035mm thick.

Fig. 5 (d) shows the final film cooling effectiveness distribution after in-situ calibrating the IR with the seed gas measurements. At the positions of the wall taps, η_{final} equals $\eta_{SG,}$ and between the taps, the IR data is offset according to the $\Delta\eta_{in\text{-}situ}$ distribution. The final film cooling results inherit the key advantages of both techniques: The high spatial resolution from the IR technique and the robustness and accuracy from the seed gas technique.

The longitudinal film cooling streaks are now clearly visible from the hub cavity exit until far downstream into the TCF passage, where the pressure taps would have been too coarse to detect them using seed gas alone.

Fig. 6 shows the individual film cooling effectiveness of the FWD and the AFT hub purge flows. Please note that the value ranges of the FWD and AFT contour plots are significantly different.

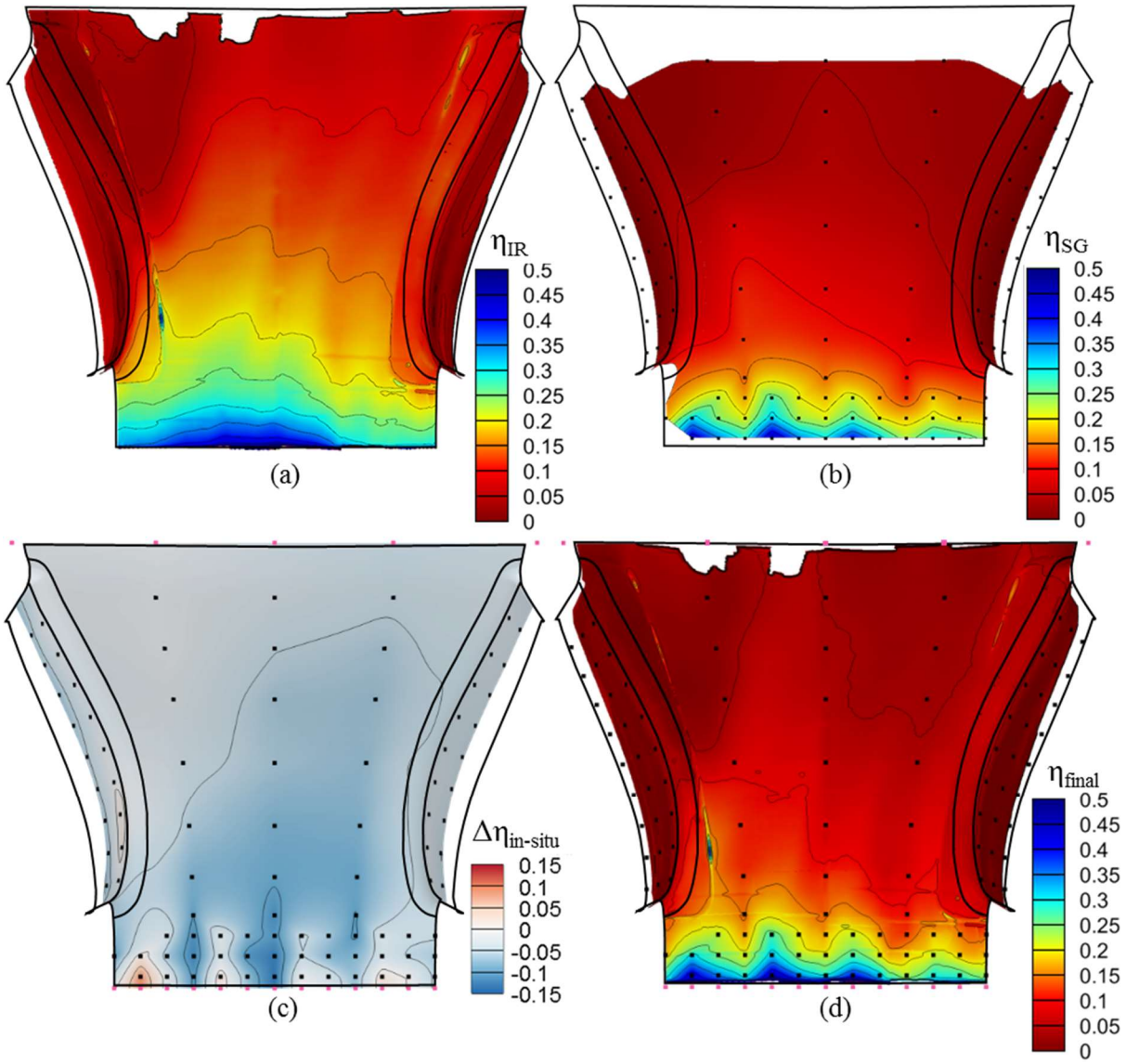

Fig. 5 (a) Purge film cooling effectiveness from IR technique, (b) from seed gas concentration technique, (c) in-situ offset, (d) final purge film cooling effectiveness

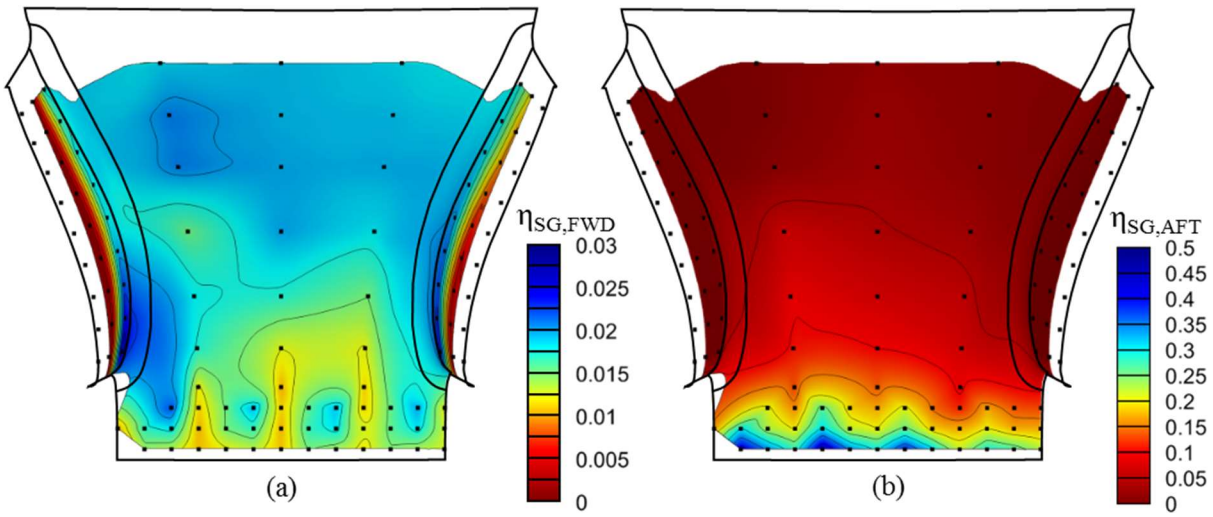

Fig. 6 Single purge film cooling effectiveness from seed gas technique of (a) FWD and (b) AFT purge flow

The cooling share of the FWD purge flow on the hub and the strut surfaces in the TCF is virtually negligible, as the film cooling effectiveness is always below 0.03. As the FWD hub purge flow passes through the rotor, it mixes almost completely with the main flow. Still, it is interesting that the FWD film cooling effectiveness is low in regions where the AFT film cooling effectiveness is high and vice versa. This is because the AFT purge flow is injected below the FWD purge flow and displaces the FWD purge flow from the surface. Since the film cooling effect of the FWD purge flow is negligibly low, the film cooling distribution of the AFT purge flow in Fig. 6 (b) is almost identical to the combined seed gas film cooling effectiveness in Fig. 5 (b).

5. UNCERTAINTY

Fig. 7 gives the uncertainties of both measurement techniques. The uncertainty of the infrared technique is taken from Jagerhofer et al. [22] and is thoroughly explained and discussed in Jagerhofer et al. [24]. The uncertainty of the seed gas measurements is taken from Patinios et al. [18] and thoroughly discussed there. Both uncertainty curves were calculated according to the *guide to the expression of uncertainty in measurement* [28] and are given as 95% confidence intervals.

The seed gas technique is nearly one magnitude more accurate than the infrared technique, which further justifies using the seed gas concentration measurements as in-situ calibration ground truth. The uncertainty of the final film cooling effectiveness, η_{final}, equals the seed gas uncertainty at the position of the wall taps. In between the wall taps, the uncertainty is slightly higher, whereas the uncertainty of the infrared technique can be considered the worst-case upper limit.

6. SUMMARY AND CONCLUSIONS

This work presented a novel hybrid approach to film cooling measurements in turbomachinery that delivers high spatial resolution, high accuracy and robustness against thermal disturbances. The combination of a heat and a mass transfer method makes it possible to benefit from the strengths of both techniques. This approach is suitable for stationary engine components with multiple coolant or purge injections, including injections from rotating wheelspace cavities.

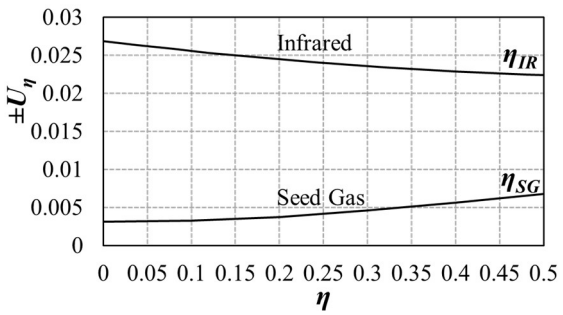

Fig. 7 Uncertainty of η as function of η (from [22]**)**

The capabilities of this hybrid approach were demonstrated in an HPT-TCF-LPT vane test vehicle operated under Mach-similarity in a continuously operating cold-flow test facility. The investigated film cooling sources were the FWD and AFT hub purge flows of an aerodynamically engine-representative HPT. The film cooling effectiveness of these purge flows was measured on the downstream TCF hub and the strut surfaces.

The IR technique comprises a multi-step pre-calibration followed by an in-situ calibration with surface thermocouples. A high TRL facility, as described above, usually harbours inevitable error sources and obstacles for a flawless implementation of a thermal measurement technique. For instance, the purge flows heat up as they radially pass through the rotating wheelspace cavity due to viscous dissipation, or ingress and re-egress of the main flow in the no purge case falsifies the baseline temperature measurements.

The seed gas concentration technique works by seeding the two purge flows with different foreign gases and analyzing gas samples drawn from static wall pressure taps. By using two different foreign gases, the individual cooling share of the FWD and the AFT purge flows is also readily accessible. The seed gas concentration technique is not susceptible to any of the thermal error sources mentioned above. The pressure tap density is the only limiting factor of this point-wise technique.

By in-situ calibrating the full surface coverage IR results with the point-wise seed gas results, a film cooling effectiveness field is obtained, that has the same spatial resolution as the IR technique, but also the same accuracy and robustness as the seed gas technique. Only by combining both techniques with the herein described approach, film cooling data was obtained that is undistorted, spatially fully resolved and, most importantly, correct.

ACKNOWLEDGMENTS

This work has been carried out in collaboration with GE Aerospace Munich and MTU Aero Engines AG, as part of the research project LuFo V-3 OptiTCF (contract no. FKZ 20T1705B) funded by the German ministry of industry BMWi.

REFERENCES

[1] D. G. Bogard and K. A. Thole, “Gas Turbine Film Cooling,” *Journal of Propulsion and Power*, vol. 22, no. 2, pp. 249–270, Mar. 2006, doi: 10.2514/1.18034.

[2] J. A. Scobie, F. P. Hualca, M. Patinios, C. M. Sangan, J. Michael Owen, and G. D. Lock, “Re-Ingestion of Upstream Egress in a 1.5-Stage Gas Turbine Rig,” *Journal of Engineering for Gas Turbines and Power*, vol. 140, no. 7, p. 072507, Jul. 2018, doi: 10.1115/1.4038361.

[3] D. D. Hänni *et al.*, “Purge flow effects on rotor hub endwall heat transfer with extended endwall contouring into the disk cavity,” *J. Glob. Power Propuls. Soc.*, vol. 3, pp. 555–568, May 2019, doi: 10.33737/jgpps/109838.

[4] J. P. Sellers, "Gaseous film cooling with multiple injection stations," *AIAA Journal*, vol. 1, no. 9, pp. 2154–2156, Sep. 1963, doi: 10.2514/3.2014.

[5] J. F. Muska, R. W. Fish, and M. Suo, "The Additive Nature of Film Cooling From Rows of Holes," *Journal of Engineering for Power*, vol. 98, no. 4, pp. 457–463, Oct. 1976, doi: 10.1115/1.3446214.

[6] T. Astarita, G. M. Carlomagno, and G. M. Carlomagno, *Infrared thermography for thermo-fluid-dynamics*. in Experimental fluid mechanics. Berlin;Heidelberg: Springer, 2013. doi: 10.1007/978-3-642-29508-9.

[7] N. Abdullah, Abd. R. Abu Talib, A. A. Jaafar, M. A. Mohd Salleh, and W. T. Chong, "The basics and issues of Thermochromic Liquid Crystal Calibrations," *Experimental Thermal and Fluid Science*, vol. 34, no. 8, pp. 1089–1121, Nov. 2010, doi: 10.1016/j.expthermflusci.2010.03.011.

[8] S. K. Biswas, C. C. Pilgrim, P. Y. Sollazzo, S. Berthier, and J. P. Feist, "Thermal history paints - principles and progress," in *IET & ISA 60th International Instrumentation Symposium 2014*, Jun. 2014, pp. 1–6. doi: 10.1049/cp.2014.0538.

[9] C. Falsetti, M. Sisti, and P. F. Beard, "Infrared thermography and calibration techniques for gas turbine applications: A review," *Infrared Physics & Technology*, vol. 113, p. 103574, Mar. 2021, doi: 10.1016/j.infrared.2020.103574.

[10] M. Martiny, R. Schiele, M. Gritsch, A. Schulz, and S. Wittig, "In situ calibration for quantitative infrared thermography," in *Proceedings of the 1996 International Conference on Quantitative InfraRed Thermography*, QIRT Council, 1996. doi: 10.21611/qirt.1996.001.

[11] S. Aberle, M. Bitter, F. Hoefler, J. C. Benignos, and R. Niehuis, "Implementation of an In-Situ Infrared Calibration Method for Precise Heat Transfer Measurements on a Linear Cascade," *Journal of Turbomachinery*, vol. 141, no. 2, p. 021004, Feb. 2019, doi: 10.1115/1.4041132.

[12] G. Barigozzi, G. Franchini, A. Perdichizzi, M. Maritano, and R. Abram, "Purge flow and interface gap geometry influence on the aero-thermal performance of a rotor blade cascade," *International Journal of Heat and Fluid Flow*, vol. 44, pp. 563–575, Dec. 2013, doi: 10.1016/j.ijheatfluidflow.2013.08.012.

[13] W. M. Kays and M. E. Crawford, *Convective heat and mass transfer*, Third edition. in McGraw-Hill series in mechanical engineering. New York: McGraw-Hill, Inc, 1993.

[14] K. S. Kulkarni, U. Madanan, R. Mittal, and R. J. Goldstein, "Experimental validation of heat/mass transfer analogy for two-dimensional laminar and turbulent boundary layers," *International Journal of Heat and Mass Transfer*, vol. 113, pp. 84–95, Oct. 2017, doi: 10.1016/j.ijheatmasstransfer.2017.05.048.

[15] J.-C. Han and A. P. Rallabandi, "TURBINE BLADE FILM COOLING USING PSP TECHNIQUE," *Frontiers in Heat and Mass Transfer*, vol. 1, no. 1, Jun. 2010, doi: 10.5098/hmt.v1.1.3001.

[16] M. Jahanmiri, "Pressure Sensitive Paints: The Basics & Applications," *Chalmers University Library*, vol. Research report 2011:07, p. 35, Jun. 2011.

[17] L. J. McNamara, "Scaling Film Cooling Adiabatic Effectiveness with Mass Transfer and Thermal Experimental Techniques," Master's Thesis, Air Force Institute of Technology Wright-Patterson AFB OH, Ohio, USA, 2019. [Online]. Available: https://apps.dtic.mil/sti/citations/AD1073903

[18] M. Patinios, F. Merli, A. Hafizovic, and E. Göttlich, "The Interaction of Purge Flows With Secondary Flow Features in Turbine Center Frames," in *Volume 2C: Turbomachinery — Design Methods and CFD Modeling for Turbomachinery; Ducts, Noise, and Component Interactions*, Virtual, Online: American Society of Mechanical Engineers, Jun. 2021, p. V02CT35A002. doi: 10.1115/GT2021-58586.

[19] R. J. Goldstein and H. H. Cho, "A review of mass transfer measurements using naphthalene sublimation," *Experimental Thermal and Fluid Science*, vol. 10, no. 4, pp. 416–434, May 1995, doi: 10.1016/0894-1777(94)00071-F.

[20] S. Friedrichs and H. P. Hodson, "THE AMMONIA AND DIAZO SURFACE COATING TECHNIQUE FOR MEASURING ADIABATIC FILM COOLING EFFECTIVENESS," in *12th Symposium on Measuring Techniques for Transonic and Supersonic Flow in Cascades and Turbomachines*, 1994.

[21] M. Steiner, S. Zerobin, S. Bauinger, F. Heitmeir, and E. Göttlich, "Development And Commissioning Of A Purge Flow System In A Two Spool Test Facility," in *12th European Conference on Turbomachinery Fluid dynamics & Thermodynamics*, EUROPEAN TURBOMACHINERY SOCIETY, 2017. doi: 10.29008/ETC2017-115.

[22] P. R. Jagerhofer, T. Glasenapp, B. Patzer, and E. Goettlich, "Heat Transfer and Film Cooling in an Aggressive Turbine Center Frame," *Journal of Turbomachinery*, pp. 1–26, Sep. 2023, doi: 10.1115/1.4063515.

[23] A. K. Sinha, D. G. Bogard, and M. E. Crawford, "Film-Cooling Effectiveness Downstream of a Single Row of Holes With Variable Density Ratio," *Journal of Turbomachinery*, vol. 113, no. 3, pp. 442–449, Jul. 1991, doi: 10.1115/1.2927894.

[24] P. R. Jagerhofer, J. Woisetschläger, G. Erlacher, and E. Göttlich, "Heat transfer and film cooling measurements on aerodynamic geometries relevant for turbomachinery," *SN Appl. Sci.*, vol. 3, no. 12, p. 889, Nov. 2021, doi: 10.1007/s42452-021-04845-5.

[25] H. Schlichting and K. Gersten, *Grenzschicht-Theorie*, 10., Überarb. Aufl. Berlin Heidelberg: Springer, 2006.

[26] M. Patinios, J. A. Scobie, C. M. Sangan, J. M. Owen, and G. D. Lock, "Measurements and Modelling of Ingress in a New 1.5-Stage Turbine Research Facility," presented at the ASME Turbo Expo 2016: Turbomachinery Technical Conference and Exposition, American Society of Mechanical Engineers Digital Collection, Sep. 2016. doi: 10.1115/GT2016-57163.

[27] R. Sibson, "A brief description of natural neighbour interpolation," *Interpreting Multivariate Data*, pp. 21–36, 1981.

[28] JCGM/WG1, "Evaluation of measurement data - Guide to the expression of uncertainty in measurement, JCGM 100:2008." JCGM, 2008. Accessed: Nov. 03, 2022. [Online]. Available: https://www.bipm.org/documents/20126/2071204/JCGM_100_2008_E.pdf/cb0ef43f-baa5-11cf-3f85-4dcd86f77bd6